Capture Illusory Contours: A Level Set Based Approach *

Wei Zhu † Tony Chan ‡

Abstract

Illusory contours are intrinsic phenomena in human vision. Many methods have been proposed to identify illusory contours. In this paper, we present a level set based variational model to capture a typical class of illusory contours such as Kanizsa triangle. The model consists of two parts: the first part drives the zero level set to the inside desired solid boundaries and keeps it sticking to the L-junctions while the second one employs the Euler's Elastica to complete the missing boundaries in a curvature continuity and short length way which has been shown to conform with human perception. The illusory contour is just the limit zero level curve. The listed experiments, including classical ones such as Kanizsa triangle and square, validate our model.

1. Introduction

Illusory contours are intrinsic phenomena in human vision. For example, if one looks at the images shown in Figure 1 (a) and (b), it is easy for him or her to recognize a triangle and a square respectively inside the images, even though part of their boundaries are missing. However, it is non-trivial for a computer vision system to recognize them.

(a) (b)

Figure 1: (a) Kanizsa triangle, (b) Kanizsa square.

Many methods have been proposed to identify illusory contours as well as explain these phenomena. They can be categorized into variational PDE based and non-PDE based methods. A typical PDE based method was provided by Sarti et al [18, 17]. In their work, they chose a fixation point inside the domain bounded by the ideal illusory contour, and constructed a surface on the whole domain on the basis of the point, then flowed the entire surface under speed law dependent on the image gradient. The flow flattened the surface except around the existing edges, and thus connected the non-existing edges to become a closed contour. The methodology of this method is novel. However, the method depends on the choice of the fixation point, and it completes the missing boundaries only by straight lines or almost straight lines, which is always insufficient to fulfill practical requirements. In [6], besides singling out the illusory contours from images, Geiger et al. also explained why some illusory contours are perceived while others are not. They detected all junctions, assigned a set of hypotheses for each of them, then selected the

*This work has been supported by ONR contract N00014-96-1-0277, NSF contract DMS-9973341 and NIH contract P20 MH65166.

†Department of Mathematics, University of California, Los Angeles, 405 Hilgard Avenue, Los Angeles, CA, 90095. E-mail: wzhu@math.ucla.edu

‡Department of Mathematics, University of California, Los Angeles, 405 Hilgard Avenue, Los Angeles, CA, 90095. E-mail: TonyC@college.ucla.edu

best image organization by minimizing a proposed energy and thus decided illusory surfaces. This method yields satisfactory results when the missing boundaries are straight lines, but fails to complete them with smooth curves. In [21], we employed the shape information to identify illusory contours. We first assumed the shape determined by the goal illusory contour was known, then we searched for the best contour with the prescribed shape which just located on the goal illusory contour. This model is easy to implement and can identify some illusory contours which are not applicable for other methods since it deals with shape information. But this model depends on given shape information.

In this paper, we propose a level set based variational model to capture illusory contours. The idea is as follows: we embed the candidate illusory contour as the zero level set of a level set function, and then update the level set function in the way such that its zero level will steer to the inside desired solid boundaries while preserving the continuity of its curvature and short length along the missing boundaries. Our model can be applied to a typical class of illusory contours such as Kanizsa triangle.

The paper is organized as follows. In section 2, Sarti et al's PDE based method [18] is reviewed. In section 3, we propose a level set based variational model as well as the numerical algorithm. Numerical results are be presented in section 4, including some classical illusory contours. Finally, a conclusion is made in section 5.

2. Sarti et al's method for completing missing boundary

In this section, we will review Sarti et al's method which is related to our work. In [18], Sarti et al proposed a PDE based model to capture illusory contours, whose methodology is different from many other combinatorial or statistical methods.

Let $I : \Omega \to \mathbf{R}$ be an image defined on a rectangle Ω. Firstly, Sarti et al built a representation called the "law primal sketch" to detect the intensity changes and vision cues such as orientation of structures and T-junctions. Specifically, they consider an edge indicator as follow:

$$\begin{aligned} g(x,y) &= \frac{1}{1+(|\nabla G_\sigma(x,y) \star I(x,y)|/\beta)^2} \\ G_\sigma(\xi) &= \frac{exp(-(|\xi|/\sigma)^2)}{\sigma\sqrt{\pi}}, \end{aligned} \tag{1}$$

where β and σ are scale parameters which determines the minimal size of the details to be detected. Thus, the value g will be close to 0 in the regions where the image intensity changes significantly, i.e., the boundaries, and will be close to 1 in homogeneous regions.

Secondly, they consider a surface $S : (x, y) \to (x, y, \Phi(x, y))$ which is also defined on the domain Ω, and then construct an energy on the function Φ by incorporating the edge indicator function g. The energy reads:

$$\int_\Omega g(x,y)\sqrt{1+\Phi_x^2+\Phi_y^2}dxdy, \tag{2}$$

and then the evolution equation for Φ is:

$$\frac{\partial \Phi}{\partial t} = g\frac{(1+\Phi_x^2)\Phi_{yy} - 2\Phi_x\Phi_y\Phi_{xy} + (1+\Phi_y^2)\Phi_{xx}}{1+\Phi_x^2+\Phi_y^2} + (g_x\Phi_x + g_y\Phi_y). \tag{3}$$

Due to the incorporation of the edge indicator g, we may see equation (2) as a weighted surface area of the surface S on Ω. As Φ is updated according to (3), the surface will become flat for most homogeneous regions in which g takes the value 1. However, on the existing edges, the sharp of the surface can be allowed because g takes the value 0. In this way, if the initial surface is chosen appropriately, the steady state surface will possess several flat surfaces, one of which can be used to identify the illusory contours.

In fact, the choice of the initial surface is crucial to this method. To this end, Sarti et al first chose a fixation point inside the the region bounded by the goal illusory contour, then set up an initial surface on the basis of the point. For example, they chose the initial Φ to be α/D, where D is the distance function from the fixation point and α is a scaling factor. With this initial surface, the flow (3) will flatten the surface as well as sharpen it on the existing boundaries and thus connect the missing boundaries. Then the illusory contour can be identified as the boundary of the high level stage of the surface.

The idea of the method is novel and it can be applied to identify illusory contours efficiently. However, as for completing missing boundaries, the model privileges straight lines or little curved ones, which may be not desirable for many illusory contours. As discussed in [18], it can be seen that around the sharp surface, or the illusory contours, the spatial derivatives will be very large, i.e., $|\Phi_x|, |\Phi_y| \gg 1$. Thus, the flow (3) approximates to

$$\frac{\partial \Phi}{\partial t} \approx g\frac{\Phi_x^2\Phi_{yy} - 2\Phi_x\Phi_y\Phi_{xy} + \Phi_y^2\Phi_{xx}}{\Phi_x^2 + \Phi_y^2} + (g_x\Phi_x + g_y\Phi_y). \tag{4}$$

Then the first term is nothing but $g\kappa(\Phi)|\nabla\Phi|$, where $\kappa(\Phi) = \nabla \cdot (\nabla\Phi/|\nabla\Phi|)$ represents the curvature of the level curve. Moreover, due to $g = 1$ on the completed boundaries, the first term becomes $\kappa(\Phi)|\nabla\Phi|$, which will straighten the curves. This fact verifies that the model prefers using straight or almost straight lines to complete the missing boundaries.

3. Our model

In this section, we will present a level set based variational model to identify illusory contours as well as a numerical algorithm.

Basically, we evolve a level set function such that its zero level set locates the goal illusory contour. To this end, two problems need to be considered. One is how to drive the zero level set to the desired solid boundaries, and the other is how to complete the missing boundaries. For the first problem, we will take advantage of the distance function defined according to the boundaries of the objects inside the image. We thus define on the zero level set an integral which measures the distance to the boundaries of the objects. Minimizing this functional will drive the zero level set to the solid boundaries. For the second problem, to remedy the inability of Sarti et al's method to complete missing boundaries using curves of complicated shape, we will employ the Euler's Elastica to restore the missing boundaries. The idea of using the Euler's Elastica is that it permits arbitrary smooth curves for the illusory parts instead of only straight or almost straight lines. In the following, we will detail our model.

3.1. Driving the zero level set to the desired solid boundaries of objects

In this subsection, we consider the problem of driving the zero level set to the desired solid boundaries of objects only.

Let $u : \Omega \to R$ be an image defined on the domain Ω. Since we mainly the problem of how to identify illusory contours, we consider in this paper only binary images, i.e., u takes only two distinct values in Ω. For convenience, let's assume u takes the value 1 on the objects and the value -1 on the background. Then, by solving the steady state of following Hamilton-Jacobi equation (Eikonal equation):

$$\frac{\partial d}{\partial t} = sign(u)(1 - |\nabla d|), \tag{5}$$

with $d(x, 0) = u(x)$, we get the signed distance function according to the boundaries the objects in the image.

In the following, we discuss how we develop a functional which drives the zero level set to the desired solid boundaries as well as preserves it on the boundaries.

Let ϕ be the level set function whose zero level set locates the illusory contours. Based on the distance function d, a functional which drives the zero level curve to the solid boundaries can be constructed as:

$$E_1(\phi) = \int_\Omega |d|\delta(\phi)|\nabla\phi| dxdy, \tag{6}$$

where $|d|$ means the absolute value of d, and $\delta(x)$ is the derivative of the Heaviside function:

$$H(x) = \begin{cases} 1, & \text{x}\geq 0 \\ 0, & \text{x}<0, \end{cases} \tag{7}$$

in the distribution sense. The integral in (6) measures the distance from the zero level set to the solid boundaries. Thus, by minimizing (6), the zero level set can be steered to the boundaries of the objects.

On the other hand, as we just want to recognize the inside illusory contour, in other words, the region $\{(x,y) \in \Omega : \phi(x,y) > 0\}$ contains no parts of the objects, we revise the functional (6) by adding a term as follows:

$$E_1(\phi) = \int_\Omega [|d|\delta(\phi)|\nabla\phi| + \lambda H(d)H(\phi)]dxdy, \tag{8}$$

where λ is positive parameter.

Then, the Euler-Lagrange equation for (8) reads:

$$\frac{\partial\phi}{\partial t} = \delta(\phi)\nabla|d| \cdot \frac{\nabla\phi}{|\nabla\phi|} + \delta(\phi)|d|\nabla \cdot (\frac{\nabla\phi}{|\nabla\phi|}) - \lambda\delta(\phi)H(d). \tag{9}$$

As [2, 20], we replace $\delta(\phi)$ by $|\nabla\phi|$, it reads:

$$\frac{\partial\phi}{\partial t} = \nabla|d| \cdot \nabla\phi + |d||\nabla\phi|\nabla \cdot (\frac{\nabla\phi}{|\nabla\phi|}) - \lambda|\nabla\phi|H(d). \tag{10}$$

Theoretically, the minimum will be arrived when the zero level set locates on the solid boundaries including all kinds of corners such as L-junctions. This minimum is in fact not stable. Therefore, if we numerically solve the Euler-Lagrange equation (10), the situation may be different from what we expect. At the steady state, the zero level set stands on the straight solid boundaries very well, while the corners (L-junctions) is smeared. This phenomenon is demonstrated in Figure 2.

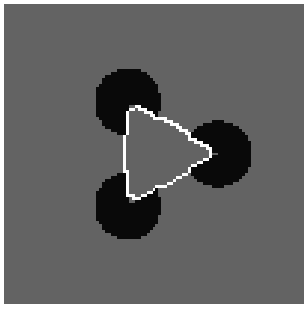

Figure 2: The white curve is the zero level set in the steady state of by solving (10). We can see the three corners are all smeared (c.f. Figure 1(a)) because the straighten term is too strong. However, the term is too weak near the missing boundaries which are not straight lines. This dilemma shows that the functional is not suitable for identifying the illusory contours with high curvature.

In fact, we can explain this phenomenon analytically and numerically. Note in the formula (10), the first term is an advection one which attracts the zero level set to the solid boundaries, while the second one is a smoothing term or straighten term, and the third term will be active only on the objects. Therefore, the first two terms will compete and thus determine the direction of moving the zero level set. At corners, the straighten term will be dominant due to their large curvature and thus they are smeared. Numerically, let's consider a simple case as shown in Figure 3.

In Figure 3, suppose the zero level set is the union of the non-negative parts of x-axis and y-axis, let us compare the two terms at the point "P". The term

$$\kappa(\phi)|\nabla\phi| = \frac{\phi_x^2\phi_{yy} - 2\phi_x\phi_y\phi_{xy} + \phi_y^2\phi_{xx}}{\phi_x^2 + \phi_y^2} \tag{11}$$

can be approximated numerically by the central differences as follows:

$$\phi_x \approx 1/2, \qquad \phi_y \approx 1/2,$$

$$\phi_{xx} \approx -1/h, \qquad \phi_{yy} \approx -1/h, \qquad \phi_{xy} \approx 2/h,$$

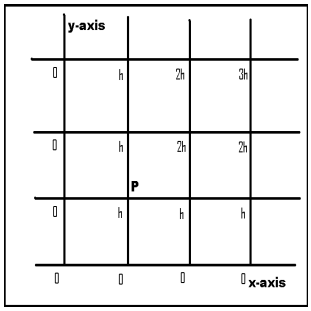

Figure 3: In this figure, the values of the level set function are shown at each grid point when the zero level set is the union of non-negative parts of x-axis and y-axis. h is the mesh size. P is a point with the coordinate (h, h).

then $|d|\kappa(\phi)|\nabla\phi| \approx -3$. On the other hand, at the point P,

$$\nabla|d| \approx (1/2, 1/2), \qquad \nabla\phi \approx (1/2, 1/2),$$

then $\nabla|d| \cdot \nabla\phi \approx 1/2$. Therefore, by (10), $\frac{\partial\phi}{\partial t}(P) = 1 - 3 = -2 < 0$, which means $\phi(P)$ will decrease, then the zero level set of ϕ will propagate across the point P. This verifies that numerically the zero level set will not be stable on the desirable solid boundaries where the curvature is very large.

Both of these facts show that the flow (10) can not fulfil what we may expect, that is, the zero level set sticks to the solid boundaries with higher curvature very well. To overcome this difficulty, we would like to incorporate the curvature of the distance function d into the functional (8). To this end, we propose a new functional as follows:

$$\begin{aligned} E_1(\phi) &= \int_\Omega [(1 + \mu\kappa^+(d))|d|\delta(\phi)|\nabla\phi| \\ &\quad +\lambda H(d)H(\phi)]dxdy, \end{aligned} \tag{12}$$

where λ, μ are tuning parameters, and $\kappa^+(d) = max(\nabla \cdot (\nabla d/|\nabla d|), 0)$.

Let us explain why we choose $\kappa^+(d)$ instead of $\kappa(d)$ and $|\kappa(d)|$. In fact $\kappa(d)$ will be positive for concave corners (L-junctions) and negative for convex corners shown in Figure 4 (Note that d is positive in the objects). For the concave corners case, just as what we calculated above, there is a competition between the two terms, i.e., advection and straighten one. The straighten term always defeats the advection term, and thus the zero level set fails to stick to the solid boundary. However, for the convex corners cases, the sign of the two terms will be the same, and both of them drive the zero level set to the solid boundary. The choice of $|\kappa(d)|$ will alleviate the function of the strengthen term especially near the concave corners where the missing boundaries will be completed.

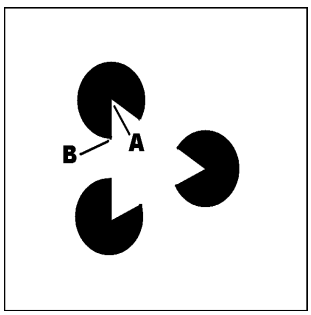

Figure 4: In this figure, the point A is a concave point where the curvature $\kappa(A)$ is positive, and the point B is convex at which the curvature $\kappa(B)$ is negative.

Moreover, in the functional (12), since we only need the term $\kappa^+(d)$ to be active around the boundaries of the

objects, we multiply the term by a C^1 differentiable cut off function $C(x)$. For example, $C(x)$ can be chosen as:

$$C(x) = \begin{cases} 1, & |x| \le \varepsilon; \\ (|x| - 2\varepsilon)^2(2|x| - \varepsilon)/\varepsilon^3, & \varepsilon < |x| \le 2\varepsilon; \\ 0, & |x| > 2\varepsilon, \end{cases} \tag{13}$$

where ϵ is a small constant. In the experiments, we always choose $\epsilon = 2h$, and h is the spatial mesh size.

Consequently, the functional (12) becomes:

$$E_1(\phi) = \int_\Omega [(1 + \mu C(d)\kappa^+(d))|d|\delta(\phi)|\nabla\phi| + \lambda H(d)H(\phi)]dxdy. \tag{14}$$

This new functional drives the zero level set of ϕ to the inside desired solid boundaries, and the zero level curve will be stable on the concave corners, which are always the key vision cues for identifying illusory contours.

Remark : In contrast to the functional (8), we substitute the term $|d|\delta(\phi)|\nabla\phi|$ for $[1 + \mu C(d)\kappa^+(d)]|d|\delta(\phi)|$ in (14). It means that we impose more weight for concave points so that the strength for steering the zero level set to them is much enforced. In some sense, the functional (14) is reasonable because these concave solid boundary points provide more vision cues for identifying the illusory contours.

3.2. Incorporating Euler's Elastica to integrate the missing boundaries

In the previous section, we discuss how to drive the zero level set to the desired solid boundaries and stick to them especially for concave boundary points. And no particular constraints are imposed on the remain parts of the zero level set which are supposed to complete the missing boundaries. In this section, we utilize Euler's Elastica to control this part of boundaries. The point is: the missing boundaries are assumed to be the ones which connect the desired solid boundaries by preserving the continuity of the curvature and the short length.

Let's review Euler's Elastica sketchily. More details can be found in [8, 2].

A curve Γ is said to be $Euler's elastica$ if it is the equilibrium curve of the elasticity energy:

$$E_2(\gamma) = \int_\gamma (a + b\kappa^2)ds, \tag{15}$$

where ds denotes the arc length element, $\kappa(s)$ the scalar curvature and a, b are two positive parameters.

In a level set function based setting, that is, the curve γ is embed as the zero level set of a function ϕ defined in the domain Ω, (15) can be rewritten as follows:

$$E_2(\phi) = \int_\Omega [a + b(\nabla \cdot (\frac{\nabla\phi}{|\nabla\phi|}))^2]|\nabla\phi|\delta(\phi)dxdy. \tag{16}$$

In summary, by combining (14) and (16), the functional for identifying the illusory contours reads:

$$\begin{aligned} E(\phi) &= E_1(\phi) + E_2(\phi) \\ &= \int_\Omega \{[(1 + \mu C(d)\kappa^+(d))|d|\delta(\phi)|\nabla\phi| + \lambda H(d)H(\phi)] \\ &\quad + [a + b(\nabla \cdot (\frac{\nabla\phi}{|\nabla\phi|}))^2]|\nabla\phi|\delta(\phi)\}dxdy. \end{aligned} \tag{17}$$

With the Euler's Elastica, we can integrate the missing boundaries in a smooth way, that is, if the tuning parameters a, b are chosen appropriately, there will be no salient jumps of curvature at the desired solid end points to which the missing boundaries are connected. This will be shown in the experiments.

3.3. Numerical Algorithm

In this section, we will discuss the Euler-Lagrange equation about ϕ according to the model (17), and then the numerical algorithm.

To be clear, we consider $E_1(\phi)$ and $E_2(\phi)$ separately.

For $E_1(\phi)$, the Euler-Lagrange equation reads:

$$\begin{aligned}\frac{\partial E_1}{\partial \phi} &= -\delta(\phi)\{\nabla[(1+\mu C(d)\kappa^+(d))|d|]\cdot\frac{\nabla\phi}{|\nabla\phi|} \\ &\quad +[1+\mu C(d)\kappa^+(d)|d|]\nabla\cdot(\frac{\nabla\phi}{|\nabla\phi|})-\lambda H(d)\},\end{aligned} \tag{18}$$

which can be derived in a standard way.

For $E_2(\phi)$, the derivation for the Euler-Lagrange equation can be found in [2], and which reads:

$$\frac{\partial E_2}{\partial \phi} = -\nabla\cdot\overrightarrow{V}, \tag{19}$$

where

$$\overrightarrow{V} = \delta(\phi)\{(a+b\kappa^2)\overrightarrow{n}-\frac{2b}{|\nabla\phi|}\frac{\partial(\kappa|\nabla\phi|)}{\partial\overrightarrow{t}}\overrightarrow{t}\},$$

and $\overrightarrow{n}=\nabla\phi/|\nabla\phi|$, $\overrightarrow{t}=(-\phi_y/|\nabla\phi|,\phi_x/|\nabla\phi|)$, $\kappa=\nabla\cdot(\nabla\phi/|\nabla\phi|)$.

Then, by combining (18) and (19) and replace $\delta(\phi)$ by $|\nabla\phi|$, we have the gradient descent equation as follows:

$$\begin{aligned}\frac{\partial\phi}{\partial t} &= \nabla[(1+\mu C(d)\kappa^+(d))|d|]\cdot\nabla\phi-\lambda H(d)|\nabla\phi| \\ &\quad +[1+\mu C(d)\kappa^+(d)|d|]|\nabla\phi|\nabla\cdot(\frac{\nabla\phi}{|\nabla\phi|})+|\nabla\phi|\nabla\cdot\overrightarrow{V}.\end{aligned} \tag{20}$$

In the experiments, first, we calculate the signed distance function d by solving (5) with the standard method which can be found in Peng et al [14] , then obtain the curvature $\kappa(d)$ and the gradient of $(1+\mu C(d)\kappa^+(d))|d|$ at each grid point.

In the following, we will discuss how to choose the discrete form for each term in the equation (20).

In fact, choosing the discrete form of the first two terms is subtle. We follow the idea discussed in Osher and Fedkiw's book [10]. The key point is how to determine the value of ϕ_x and ϕ_y.

For simplicity, denote $A=(1+\mu C(d)\kappa^+(d))|d|$.

Let

$$H(\phi_x,\phi_y) = \nabla A\cdot\nabla\phi-\lambda H(d)|\nabla\phi|, \tag{21}$$

then the partial derivatives to the two augments are:

$$H_1(\phi_x,\phi_y) = A_x-\lambda H(d)\frac{\phi_x}{|\nabla\phi|}, \tag{22}$$

$$H_2(\phi_x,\phi_y) = A_y-\lambda H(d)\frac{\phi_y}{|\nabla\phi|}, \tag{23}$$

where $A_x=\partial A/\partial x$, $A_y=\partial A/\partial y$. Since we do re-initialization for ϕ frequently in the experiments, we may assume $|\nabla\phi|=1$, the above two derivatives can be rewritten as:

$$H_1(\phi_x,\phi_y) = A_x-\lambda H(d)\phi_x, \tag{24}$$

$$H_2(\phi_x,\phi_y) = A_y-\lambda H(d)\phi_y, \tag{25}$$

To determine the values of ϕ_x and ϕ_y, we set $\phi_x^+=(\phi_{i+1,j}-\phi_{i+1,j})/h$ and $\phi_x^-=(\phi_{i,j}-\phi_{i-1,j})/h$. Then we check the following cases:

Case I: $H(d)>0$

case 1: if $H_1(\phi_x^+,\phi_y)>0$, $H_1(\phi_x^+,\phi_y)>0$, then $\phi_x=\phi_x^-$,

case 2: if $H_1(\phi_x^+, \phi_y) < 0$, $H_1(\phi_x^+, \phi_y) > 0$, then $\phi_x = A_x/(\lambda H(d))$,
case 3: if $H_1(\phi_x^+, \phi_y) > 0$, $H_1(\phi_x^+, \phi_y) < 0$, then
case 3a: $\phi_x^- \le \phi_x^+$,
if $H_1(\phi_x^-, \phi_y) < H_1(\phi_x^+, \phi_y)$, then $\phi_x = \phi_x^-$, else $\phi_x = \phi_x^+$,
case 3b: $\phi_x^- > \phi_x^+$,
if $H_1(\phi_x^-, \phi_y) < H_1(\phi_x^+, \phi_y)$, then $\phi_x = \phi_x^+$, else $\phi_x = \phi_x^-$,
case 4: if $H_1(\phi_x^+, \phi_y) < 0$, $H_1(\phi_x^+, \phi_y) < 0$, then $\phi_x = \phi_x^+$,

Case II: $H(d) = 0$
case 1: if $A_x > 0$, then $\phi_x = \phi_x^+$,
case 1: if $A_x \le 0$, then $\phi_x = \phi_x^-$.

Similarly, we can chose the value ϕ_y according to the same principle.

For the third term, we use the central difference, that is,

$$\phi_{xx} \approx \frac{\phi_{i+1,j} - 2\phi_{i,j} + \phi_{i-1,j}}{h^2},$$

$$\phi_{yy} \approx \frac{\phi_{i,j+1} - 2\phi_{i,j} + \phi_{i,j-1}}{h^2},$$

$$\phi_{xy} \approx \frac{\phi_{i+1,j+1} + \phi_{i-1,j-1} - \phi_{i+1,j-1} + \phi_{i-1,j+1}}{4h^2},$$

and

$$\phi_x \approx \frac{\phi_{i+1,j} - \phi_{i-1,j}}{2h},$$

$$\phi_y \approx \frac{\phi_{i,j+1} - \phi_{i,j-1}}{2h}$$

to approximate

$$\kappa(\phi)|\nabla\phi| = \frac{\phi_x^2\phi_{yy} - 2\phi_x\phi_y\phi_{xy} + \phi_y^2\phi_{xx}}{\phi_x^2 + \phi_y^2}.$$

For the last term, details can be found in [2].

Since the zero level set of ϕ is the only thing what we want, we employ a local level set method [14] to solve (20) to reduce the computation. This point is: instead of solving the following equation:

$$\frac{\partial\phi}{\partial t} + u_n|\nabla\phi| = 0, \tag{26}$$

they solve

$$\frac{\partial\phi}{\partial t} + c(\phi)u_n|\nabla\phi| = 0, \tag{27}$$

where

$$c(x) = \begin{cases} 1, & |x| \le \beta; \\ (|x| - \gamma)^2(2|x| + \gamma - 3\beta)/(\gamma - \beta)^3, & \beta < |x| \le \gamma; \\ 0, & |x| > \gamma, \end{cases} \tag{28}$$

where β and γ are two positive constants. In the computation, we choose $\beta = 3h$, $\gamma = 6h$, and h is the spatial mesh size.

Remark : This local level set method speeds up the process remarkably, since it only updates the goal level set function ϕ inside a tube around its zero level set. It changes a two-dimensional problem to a one-dimensional one in some sense. In fact, utilizing this method is crucial. Note that the evolution equation (20) is actually a forth-order one if the parameter $b \neq 0$, therefore by the CFL condition, the time step size should be proportional to the forth power of the spatial step size, i.e., $dt \sim dx^4$.

4. Numerical Experiments

In this section, we present some experiments including Kanizsa triangle and square.

For all the experiments listed here, the sizes of the images are 100×100. Basically, it takes less than $10^3 \sim 10^4$ iterations when the missing parts are straight lines, i.e., $b = 0$, and $10^6 \sim 10^7$ iterations for the curved case where $b \neq 0$. Moreover, we may choose the initialization of ϕ freely— we only require its zero level set contains all the objects in the image.

Figures 5 and 6 show the classical illusory contours—Kanizsa triangle and square. In these two examples, we only need to choose $b = 0$ in (20) because the missing boundaries are actually straight lines by the continuity of the curvature, on the other hand, a nonzero choice of b will not affect the final results. Choosing $b = 0$ makes the evolution equation (20) become a second order instead of forth order equation, which speeds the evolution process remarkably. In these two examples, the corners are preserved very well while the missing parts are integrated by straight lines.

Figure 7 shows a general four-edged shape. As in Figure 5 and 6, we also chose $b = 0$ in (20). As the previous examples, the corners are preserved very well.

The above three examples verify that our model can be applied to the cases that the missing boundaries are straight lines. As described in the model, on one hand, the zero level set of the goal function is steering to the desired solid boundaries, on the other hand, it also sticks to the corners even though the curvature there could be very large in computational sense, since the curvature at the corners does not exist theoretically.

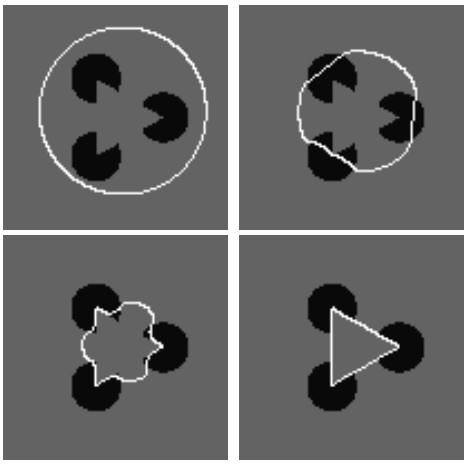

Figure 5: This image is the classical Kanizsa Triangle. The evolution process is listed with four figures from top to bottom and left to right. The parameters chosen for this example are: $\lambda = 3.0$, $\mu = 15.0$, $a = 0.5$, $b = 0$.

The next two examples (Figure 8 and 9) demonstrate that our model is also capable of completing the missing boundaries by curves. We choose nonzero b in (20) here. As in the previous examples, the zero level set is driven to the desired solid boundaries. Moreover, it completes the missing boundaries by a short smooth curve along which there are no salient jumps in the curvature, i.e., the curvature is continuous.

In Figure 10, we compare the result with that of in Figure 8 by choosing $a = 0$, $b = 0$. One may find the missing boundaries are completed by straight lines, instead of smooth curves as in Figure 8. This shows the Euler's Elastica does preserve the continuity of curvature.

In the next example (Figure 11), we present a group of final results for the same image with different choice of the parameter b. We find that with the same choice of the parameter a, the larger the parameter b, the less the change of the curvature along the missing parts.

5. Conclusions

In this paper, we propose a level set based variational model to capture the illusory contours. We embed the candidate illusory contour as the zero level curve of a level set function, and construct a functional of the level set

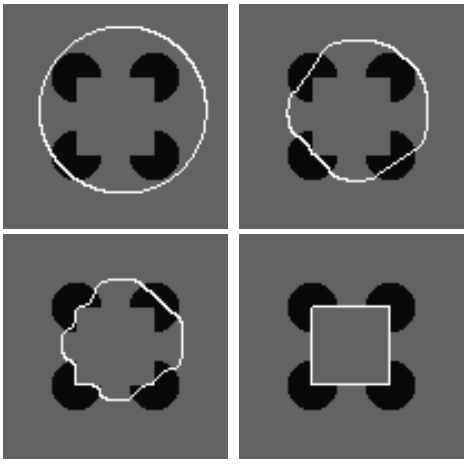

Figure 6: This image is the classical Kanizsa Square. The evolution process is listed with four figures from top to bottom and left to right. The parameters chosen for this example are: $\lambda = 3.0$, $\mu = 15.0$, $a = 0.5$, $b = 0$.

function. By minimizing the functional, the zero level curve will be driven to the inside desired solid boundaries, be stable on them especially on the corners (L-junctions) and will complete the missing boundaries by preserving the continuity of curvature and preferring a short length. We apply our model to several images whose missing boundaries are completed smoothly according to the continuity of curvature.

Acknowledgments

The first author would like to thank Stanley Osher for his suggestion.

References

[1] V. Caselles, R. Kimmel and G. Sapiro, *Geodesic active contours,* International Journal of Computer Vision, 22:1, PP. 61-79, 1997.

[2] T. Chan, Sung Ha Kang, and Jianhong Shen, *Euler's Elastica and Curvature Based Inpaintings,* UCLA CAM Report 01-12, 2001.

[3] T. Chan and L.A. Vese, *Active contours without edges,* IEEE Transaction on Image Processing, 10(2):266-277, February 2001.

[4] T. Chan and L.A. Vese, *A level set algorithm for minimizing the Mumford-Shah functional in image processing,* In IEEE Workshop on Variational and Level Set Methods, pages 161-168, Vancouver, CA, 2001.

[5] D. Geiger, K. Kumaran and L. Parida, *Visual Organization for Figure/Ground Separation,* IEEE Conference on Conputer Vision and Pattern Recognition, June 1996, San Francisco, CA.

[6] D. Geiger, H.K. Pao and N. Rubin, *Salient and Multiple illusory surfaces,* IEEE Computer Society Conference on Conputer Vision and Pattern Recognition, June 1998, San Barbara, CA.

[7] G. Kanizsa, *Organization in Vision: essays on Gestalt Perception,* Praeger, New York, 1979.

[8] D. Mumford, *Elastica and computer vision,* In C. L. Bajaj, editor, *Algebraic Geometry and its applications,* pages 491-506, Springer-Verlag, New York, 1994.

[9] S. Osher and J.A. Sethian, *Fronts Propagating with Curvature-Dependent Speed-Algorithm Based on Hamilton-Jacobi Formulations,* J. Comput. Phys, Vol 79, 12-49, 1988.

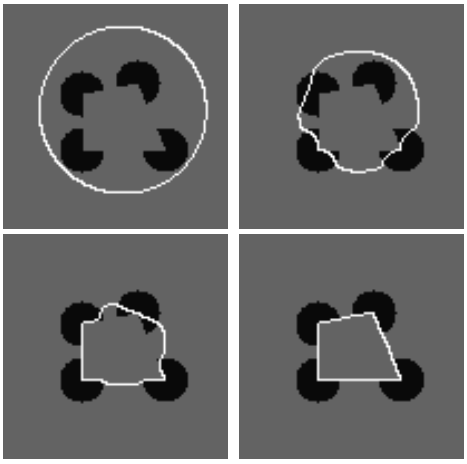

Figure 7: This image is a general four-edged shape. The evolution process is listed with four figures from top to bottom and left to right. The parameters chosen for this example are: $\lambda = 3.0$, $\mu = 15.0$, $a = 0.5$, $b = 0$.

[10] S. Osher and R. Fedkiw, *Level Set Methods and Dynamic Implicit Surfaces,* Springer-Verlag, 2002.

[11] H.K. Pao and D. Geiger, *A continuous Shape Descriptor by Orientation Diffusion,* In the 3rd International Workshop, EMMCVPR, Sep. 2001, France, pp. 544-559.

[12] H.K. Pao, D. Geiger and N. Rubin, *Meauring Convexity for Figure/Ground Separation,* In 7th International Conference on Computer Vision, Sep. 1999, Kerkyra, Greece.

[13] N. Paragios, M. Rousson and V. Ramesh, *Matching Distance Functions: A Shape-to-Area Variational Approach for Global-to-Local Registration,* European Conference in Computer Vision, Copenhangen, Denmark, 2002.

[14] Danping Peng, Barry Merriman, Stanley Osher, Hongkai Zhao, and Myungjoo Kang, *A PDE-based fast local level set method,* J. Comput. Phys, Vol 155, 410-438, 1999.

[15] S. Petry and G.E. Meyer, editors, *The Perception of illusory contours,* Springer-Verlag, New York, 1987.

[16] M. Rousson and N. Paragios, *Shape Priors for Level Set Representaions,* European Conference in Computer Vision, Copenhangen, Denmark, 2002.

[17] A. Sarti and G. Citti, *Subjective surfaces and Riemann mean curvature flow of graphs,* Acta Math. Univ. Comenianae, Vol. LXX, 1(2001), pp. 85-103, Proceedings of Algoritmy 2000.

[18] A. Sarti, R. Malladi and J.A. Sethian, *Subjective surfaces: A method for completing missing boundaries.* Proceedings of the National Academ of Sciences of the United States of America, Vol 12, N.97, page. 6258-6263, 2000.

[19] S. Ulman. *Filling in the gaps: The shape of subjective contours and a model for their generation.* Biological Cybernetics, 25:1-6, 1976.

[20] H.K. Zhao, T. Chan, B. Merriman and S. Osher, *A variational level set approach to multiphase motion.* J.Comput.Phys., 127:179-195,1996.

[21] W. Zhu, and T. Chan, *Illusory contours using shape information.* UCLA CAM Report 03-09, 2003.

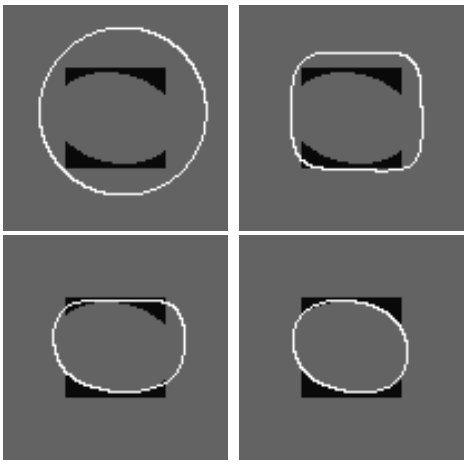

Figure 8: This image contains an illusory ellipse inside a square. The evolution process is listed with four figures from top to bottom and left to right. The parameters chosen for this example are: $\lambda = 3.0$, $\mu = 15.0$, $a = 0.01$, $b = 0.5$.

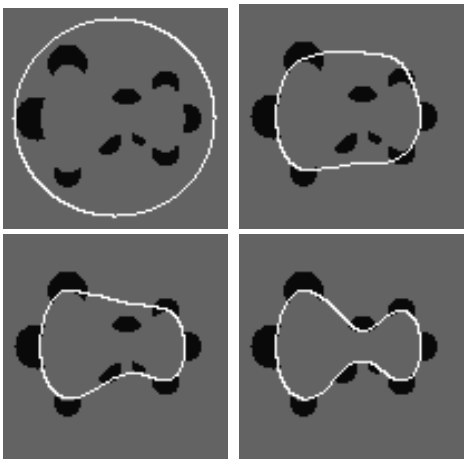

Figure 9: In this image, the illusory contour is a dumb-ring. The evolution process is listed with four figures from top to bottom and left to right. The parameters chosen for this example are: $\lambda = 3.0$, $\mu = 15.0$, $a = 0.005$, $b = 0.05$.

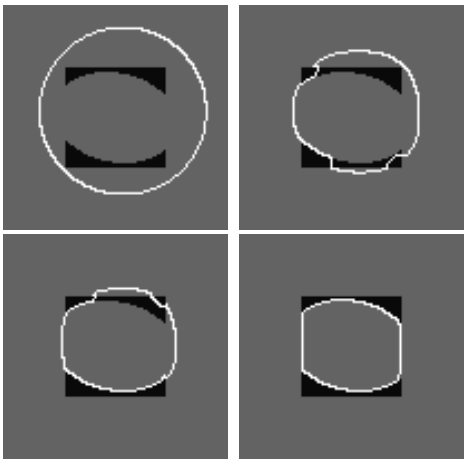

Figure 10: This image is an ellipse inside a square. The evolution process is listed with four figures from top to bottom and left to right. The parameters chosen for this example are: $\lambda = 3.0$, $\mu = 15.0$, $a = 0.01$, $b = 0$.

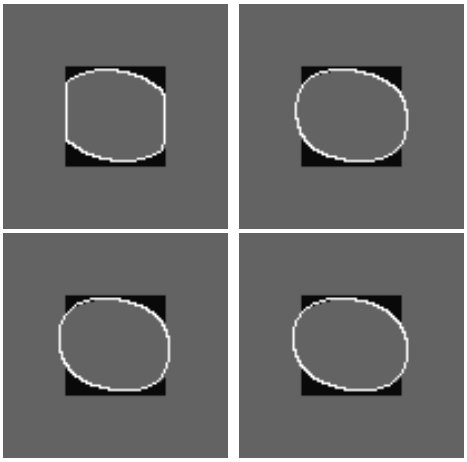

Figure 11: These images are the final results according to different choice of the parameter b and the same a. Here $a = 0.01$, and $b = 0, 0.1, 0.3, 0.5$ from top to bottom and left to right respectively.